11th World Congress on Computational Mechanics (WCCM XI)
5th European Conference on Computational Mechanics (ECCM V)
6th European Conference on Computational Fluid Dynamics (ECFD VI)
E. Oñate, J. Oliver and A. Huerta (Eds)

DIRECT AND LARGE EDDY SIMULATIONS OF NON-OBERBECK-BOUSSINESQ EFFECTS IN A TURBULENT TALL WATER-FILLED DIFFERENTIALLY HEATED CAVITY

DENIZ KIZILDAG, IVETTE RODRÍGUEZ, F. XAVIER TRIAS and ASSENSI OLIVA

Heat and Mass Transfer Technological Center (CTTC)
Universitat Politècnica de Catalunya - BarcelonaTech (UPC)
Colom 11, 08222 Terrassa, Barcelona, Spain
cttc@cttc.upc.edu

Key words: Non-Oberbeck-Boussinesq, Turbulent Natural Convection, Direct Numerical Simulation, Large Eddy Simulation.

Abstract. The present work first submits to investigation the non-Oberbeck-Boussinesq (NOB) effects in a tall water-filled differentially heated cavity by means of direct numerical simulations. The results reveal that if NOB effects are considered, the flow is no longer symmetric as the transition point moves downstream on the hot wall and upstream on the cold wall. Afterwards, the assessment of the large eddy simulation models is performed in order to test their capabilities for not only capturing the complex phenomena like transition to turbulence, turbulent mixing, and interaction between the boundary layers, but also for reproducing the NOB effects. The performance of different subgrid-scale models is assessed.

1 INTRODUCTION

The canonical differentially heated cavity (DHC) flow has been extensively studied in the literature due to its potential to model many applications of academic and industrial interest. The vast majority of the conducted studies are related with air-filled cavities (Prandtl number $Pr \approx 0.7$) considering the so-called Oberbeck-Boussinesq (OB) approximation (see, for instance [1, 2]). If the cavity is water-filled, obtaining solutions gets more complicated as the boundary layer becomes thinner [3], thus requiring finer grids to capture the smallest scales of the turbulent flow. Moreover, for water-filled cavities under practical working conditions, the OB approximation is questionable [4] as a consequence of important variations in the thermophysical properties, especially in the viscosity. Regarding the numerical studies on water filled cavities, Le Quéré's work [5] can be cited. He

studied a water-filled DHC of aspect ratio 10 on a 2D domain considering OB assumption. More recently, the non-Oberbeck-Boussinesq (NOB) effects in a tall water-filled DHC on a 2D domain at a wide range of temperature differences were studied [6] by means of direct numerical simulations (DNS). In that investigation, a substantially different flow configuration was observed beyond a temperature difference of 30 $^{\circ}C$, where NOB effects were found to be relevant.

The objective of the present investigation is twofold. First, by means of 3D DNS, the NOB effects are submitted to study in order to check the adequacy of the conclusions obtained by means of 2D hypothesis for a similar flow configuration [6]. To that end, two DNS studies of the turbulent natural convection in a DHC of aspect ratio 10 at $Ra = 3 \times 10^{11}$ and $Pr = 3.41$ (corresponding to water at 50 $^{\circ}C$) are carried out, one with OB approximation, the other considering NOB effects, for a temperature difference of $\Delta T = 80$ $^{\circ}C$ between the isothermal confining walls. Second, the assessment of different subgrid-scale (SGS) models is carried out for the configuration under study. To do this, the results obtained with the models are compared to those obtained by means of DNS for both OB and NOB hypotheses.

2 CASE DEFINITION

The turbulent natural convection submitted to study for a DHC element of height H, width W, and depth D is shown in Figure 1. The present configuration yields a height aspect ratio, $\Gamma = H/D$, of 10. The depth aspect ratio, $\Gamma_d = D/W$, is one half. The cavity is heated and cooled by means of vertical isothermal confining walls. To that end, the wall temperatures are set to $T_h = 90$ $^{\circ}C$ and $T_c = 10$ $^{\circ}C$ as shown in Figure 1. The top and bottom walls are adiabatic. No-slip condition is adopted in these horizontal and vertical confining walls, while in the depth direction periodic boundary condition is imposed.

The cavity height based Rayleigh number ($Ra = |\mathbf{g}|\beta(T_h - T_c)H^3 Pr/\nu^2$) is 3×10^{11}, and the Prandtl number ($Pr = \nu/\alpha$) is 3.41, where $\mathbf{g}$ is the gravity acceleration, β is the thermal expansion coefficient, ν is the kinematic viscosity, α is the thermal diffusivity ($\alpha = k/\rho C_p$), k is the thermal conductivity, and C_p is the specific heat. The thermophysical properties of water are calculated at the mean temperature of $T_m = (T_h + T_c)/2 = 50$ $^{\circ}C$.

3 MATHEMATICAL AND NUMERICAL MODEL FOR DNS

It is common to use the OB approximation in buoyancy driven flows, especially if the range of temperature differences is relatively low. This approach considers constant thermophysical properties except for the density in the buoyancy term, which is approximated as a linear function of temperature. Assuming the OB approximation, the governing equations read:

$$\begin{aligned} \nabla \cdot \mathbf{u} &= 0, \\ \partial_t \mathbf{u} + \mathcal{C}(\mathbf{u}, \mathbf{u}) &= \nu_m \Delta \mathbf{u} - \nabla p - \beta_m (T - T_m)\mathbf{g}, \\ \partial_t T + \mathcal{C}(\mathbf{u}, T) &= \alpha_m \Delta T, \end{aligned} \tag{1}$$

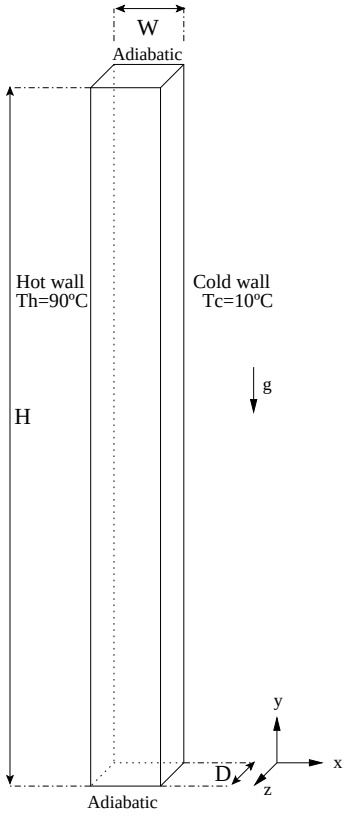

Figure 1: Geometry of the case submitted to study

where $\mathbf{u}$ denotes the velocity field, p is the kinematic pressure, and the convective term is given by $\mathcal{C}(\mathbf{u},\mathbf{v}) = (\mathbf{u}\cdot\nabla)\mathbf{v}$. The subscript m denotes that the thermophysical properties are evaluated at the mean temperature T_m. As the NOB effects are considered, the governing equations for incompressible flows can take the following form:

$$\begin{aligned} \nabla\cdot\mathbf{u} &= 0, \\ \partial_t\mathbf{u} + \mathcal{C}(\mathbf{u},\mathbf{u}) &= 2\rho_m^{-1}\nabla\cdot(\mu S(\mathbf{u})) - \nabla p + (1-\rho/\rho_m)\mathbf{g}, \\ \partial_t T + \mathcal{C}(\mathbf{u},T) &= (\rho_m C_{p,m})^{-1}\nabla\cdot(k\nabla T), \end{aligned} \tag{2}$$

where $S(\mathbf{u}) = 1/2(\nabla\mathbf{u} + \nabla\mathbf{u}^T)$. The dynamic viscosity, μ, and k are temperature dependant whereas $C_{p,m}$ and ρ_m are evaluated at the mean temperature. The differential operators have been discretized by means of a symmetry-preserving discretization [7]. The discretization of the viscous dissipation term, $2\nabla\cdot(\mu S(\mathbf{u}))$, with spatially varying dynamic viscosity can be difficult especially for high-order staggered formulations. To circumvent this problem, the following form for the viscous term

$$2\nabla\cdot(\mu S(\mathbf{u})) = \nabla\cdot(\mu\nabla\mathbf{u}) + \nabla(\nabla\cdot(\mu\mathbf{u})) - \mathcal{C}(\mathbf{u},\nabla\mu), \tag{3}$$

has been derived [8]. From a numerical point-of-view, the most remarkable property is that it can be straightforwardly implemented by simply re-using operators. Moreover, for

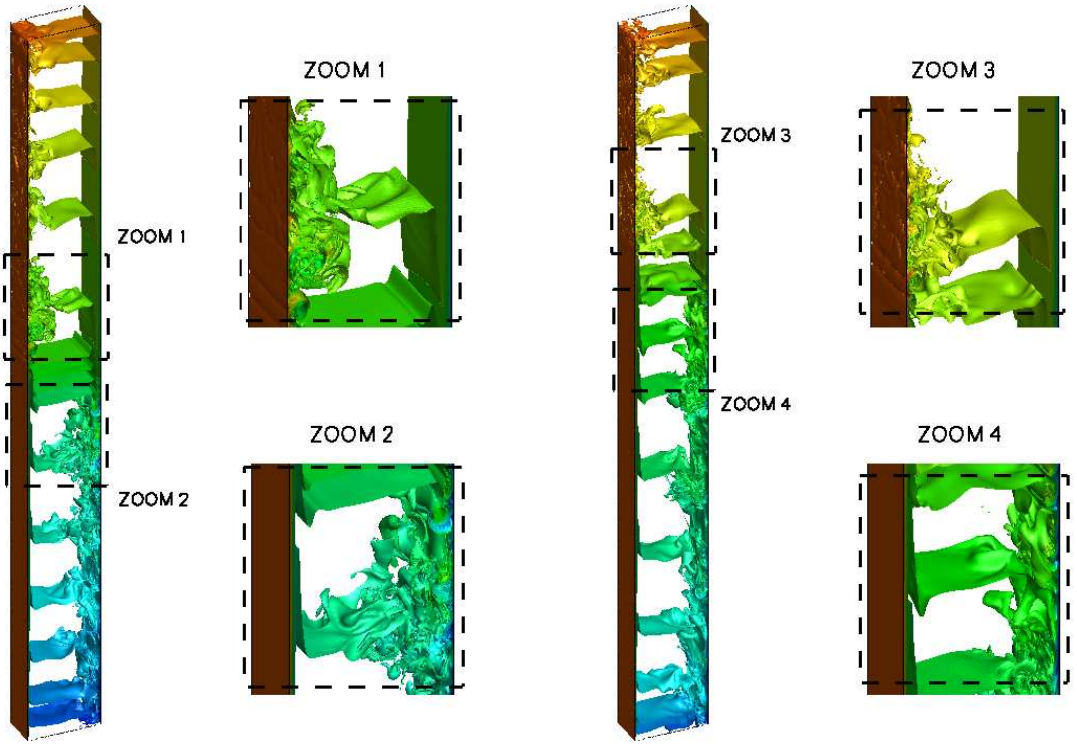

Figure 2: Representative instantaneous temperature isotherms for OB (left) and NOB (right) using DNS.

constant viscosity, formulations constructed via Eq.(3) become identical to the original formulation since the last two terms in the right-hand-side exactly vanish.

Governing equations are discretized by means of a finite volume fully conservative fourth-order scheme for spatial discretization [7] and a second order explicit scheme for time integration [9]. The pressure-velocity linkage is solved by means of an explicit finite volume fractional step procedure. The generated domain is periodic in the $z-$direction. Therefore, the system of equations is reduced to a set of 2D systems by means of a Fourier diagonalization method. These systems are solved using a Direct Schur complement-based domain Decomposition method in conjunction with a Fast Fourier Transform [10].

4 NUMERICAL METHODS FOR LES

LES are carried out by using the *Termofluids* code [11], which is a parallel unstructured object oriented code. The numerical methods are essentially the same as the ones detailed for DNS, except for using second-order conservative schemes on collocated meshes in the discretization of the governing equations for OB and NOB approximation. This kind of schemes ensure both stability and conservation of the global kinetic-energy balance on any grid, thus constituting a convenient starting point for LES-like simulations [7].

In the present work, the assessment of different SGS models is performed: the wall-

adapting large-eddy model (WALE) [12], the QR model [13], and the WALE model within a variational multiscale framework [14]. For the details of the models the reader is referred to the corresponding references.

5 NUMERICAL PARAMETERS AND RESULTS

In this section, the preliminar results obtained so far has been analyzed. In order to assure that the complex phenomena are reproduced by the numerical simulations, different meshes has been tested, while the results from only three of them are given in this work (see Table 1). Following the previous approaches for this configuration, the meshes are uniform in $y-$ and $z-$directions, while a hyperbolic function is used in the wall-normal direction (see [6] for details). For the presentation of the dimensionless results, the reference length, time, velocity, and temperature are H, $(H^2/\alpha)Ra^{-0.5}$, $(\alpha/H)Ra^{0.5}$, and $(T_h - T_c)$, respectively.

Table 1: Mesh parameters for DNS. N_x, N_y, and N_z are the number of CVs in $x-$, $y-$, and $z-$directions, respectively. N_{total} is the number of total CVs in millions. Δx_{min} is the smallest non-dimensional wall-normal distance.

Mesh	N_x	N_y	N_z	N_{total}	$\Delta x_{min}/H$
mesh A	174	702	96	11.73	1.15×10^{-4}
mesh B	140	560	64	5.02	1.44×10^{-4}
mesh C	55	511	16	0.45	4.80×10^{-4}

In Figure 2, representative instantaneous temperature isotherms are presented for both OB and NOB conditions using mesh C. Note that using the OB assumption, the temperature map is symmetric over the center of the cavity, where a highly stratified region of quasi-parallel isotherms are observed. The transition point on the hot and cold walls occurs to be bounding symmetrically this highly stratified region. When NOB effects are considered, the symmetry of the temperature isotherms is broken. The stratified region shifts upwards as a consequence of downstream transition on the hot wall and upstream transition on the cold wall. This is in agreement with the outcome of the previous work for a similar configuration on a two-dimensional domain at the same Rayleigh number[6].

In Figure 3, the mesh refinement studies of DNS using OB assumption are carried out by means of the local averaged Nusselt number, Nu, and its standard deviation. In the study, 3 meshes are used (see Table 1 for the details of the meshes). Note that the standard deviation of the local averaged Nu is an indicator of temperature fluctuations, thus pointing out the transition to turbulence. The figure shows that the solution on the coarsest mesh (mesh C), referred to as "No Model OB II" solution, deviates significantly from the solution on the intermediate mesh, "No Model OB I", as the transition trend is concerned. However, the finest mesh solution qualitatively reproduces the transition to

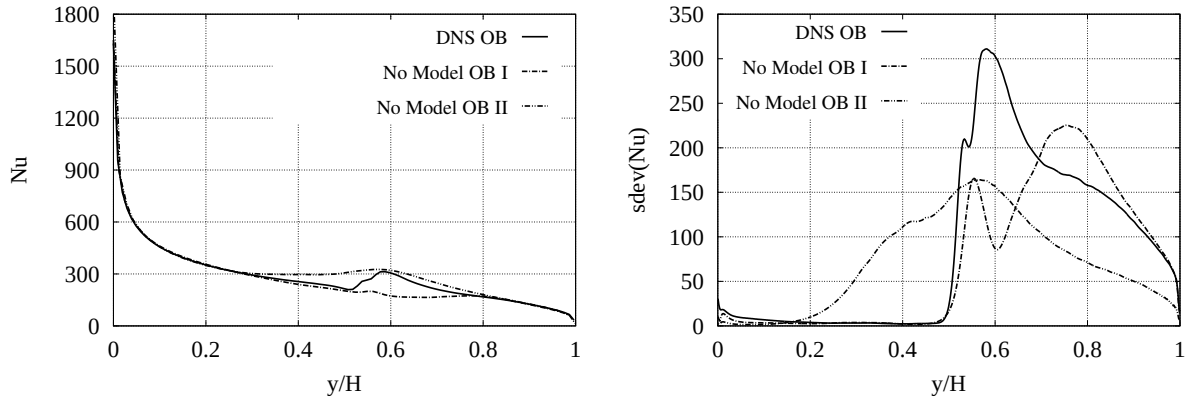

Figure 3: Mesh refinement studies for DNS using OB assumption. Local averaged Nusselt number (left) and its standard deviation (right).

turbulent phenomenon observed for the intermediate mesh. Owing to this, hereafter the solution on the finest mesh is referred to as the DNS solution.

The same meshes are used for the mesh refinement studies of DNS considering NOB effects. As anticipated from the instantaneous maps of Figure 2, the flow is not symmetric in this case, thus justifying the analysis of the previously compared quantities in the both boundary layers. It can be observed in Figure 4 that, in the vicinity of the hot wall, mesh resolution is less critical when compared with the corresponding OB case, as the coarsest "No Model NOB II" solution can qualitatively reproduce the DNS solution for a significant portion of the boundary layer. However, this is not the case in the vicinity of the cold wall (see Figure 5) where the coarsest mesh predicts premature transition. Note that for the NOB case on the cold wall, the intermediate solution can satisfactorily reproduce the behavior of the finest mesh solution.

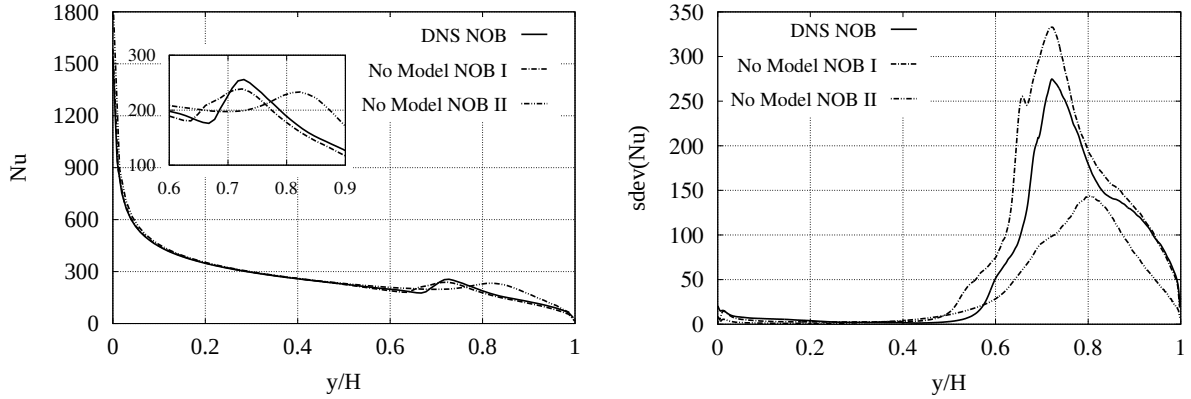

Figure 4: Mesh refinement studies for DNS considering NOB effects. Local averaged Nusselt number (left) and its standard deviation (right) on the hot wall.

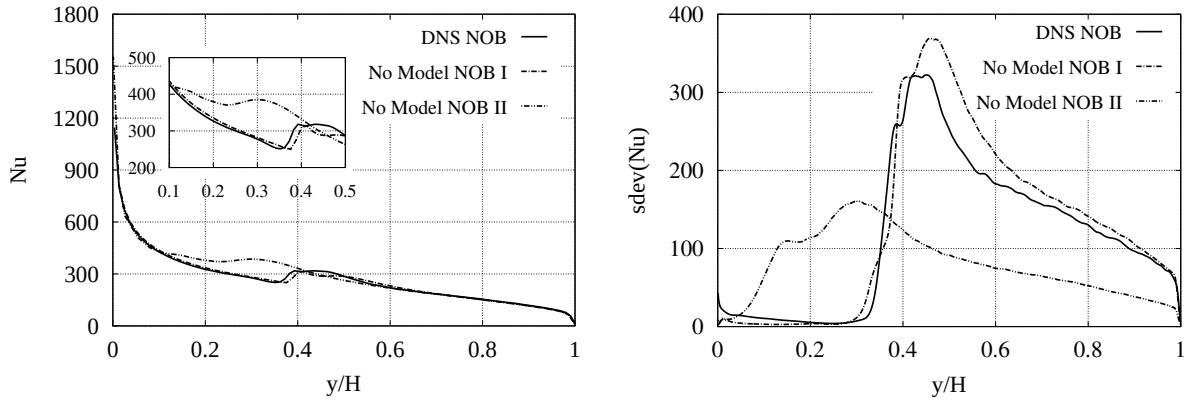

Figure 5: Mesh refinement studies for DNS considering NOB effects. ocal averaged Nusselt number (left) and its standard deviation (right) on the cold wall.

The results presented in the current work are summarized in Table 2, where the tested cases are described, the overall averaged Nusselt number, $\overline{Nu}$, and the transition point on the hot and cold walls are given. Owing to the high computational demand of DNS, a compromise between accuracy and integration time is made. Given the differences between "DNS OB" and "No Model OB I" cases, a mesh with higher resolution has to be tested to ensure confidence with the presented OB results. As for the NOB solution, the agreement in the results for the intermediate and fine meshes may indicate that the presented results do not deviate considerably from the mesh-independent solution.

Table 2: Summary of the tested cases. t_{int} is the integration time. Transition points, $x_{tr,hot}$ and $x_{tr,cold}$, are defined as the location where the standard deviation of Nu exceeds 2% of the local average value, on the hot and cold walls, respectively.

Case	Mesh	t_{int}	$\overline{Nu}$	$x_{tr,hot}/H$	$x_{tr,cold}/H$
DNS OB	Mesh A	120	283	0.48	0.48
DNS NOB	Mesh A	90	273	0.51	0.29
No Model OB I	Mesh B	240	263	0.47	0.47
No Model NOB I	Mesh B	240	272	0.45	0.28
No Model OB II	Mesh C	240	305	0.18	0.18
No Model NOB II	Mesh C	240	287	0.42	0.03

Finally in Figure 6, NOB effects are analyzed by means of previously compared quantities. The figure shows that when the NOB effects are considered, the transition point goes downstream on the hot wall, and upstream on the cold wall, as expected from the instantaneous maps.

Although not shown here, a preliminary work on the assessment of WALE has been started at the time of submission of the present document, yielding promising results. In

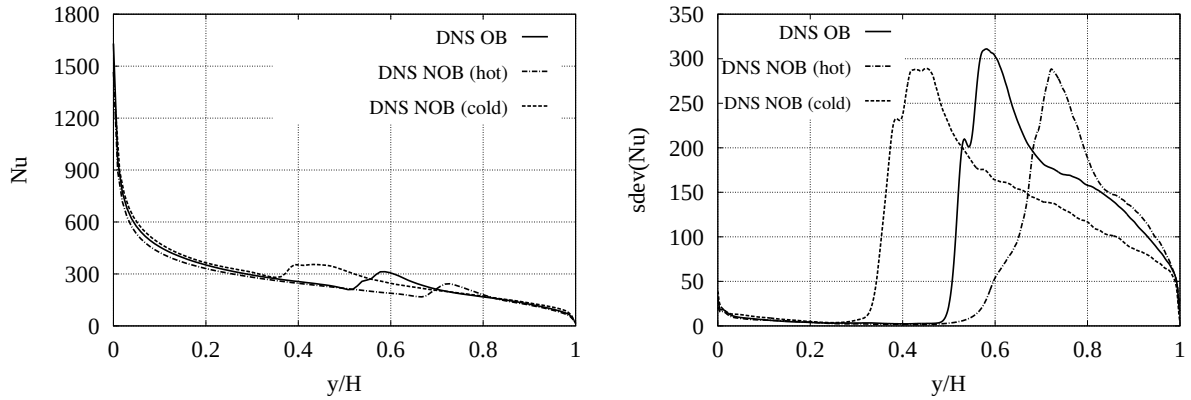

Figure 6: NOB effects obtained by DNS. Local averaged Nusselt number (left) and its standard deviation (right).

order to present a rigorous methodology on the model assessment, the mesh-independent DNS solution is required, which is the objective of the present ongoing research. Final results will be presented in the conference.

6 CONCLUSIONS

The present work first submits to investigation the NOB effects in a tall water-filled DHC on a 3D domain. To that end, two DNS are carried out, one using OB assumption, and the other considering NOB effects. The results show that as the NOB effects are considered, the flow symmetry is broken. The transition point moves downstream on the hot wall, and upstream on the cold wall. The behavior of the transition points and the upward shift of the highly stratified region are in agreement with the results presented for a similar configuration on a 2D domain [6]. Secondly, as a future work, the performance of SGS models will be assessed by means of comparison with the DNS data considering both OB and NOB conditions, once the mesh-independent results are obtained.

ACKNOWLEDGMENTS

This work has been partially supported by the Ministerio de Economía y Competitividad, Secretaría de Estado de Investigación, Desarrollo e Innovación, Spain (Ref. ENE2010-17801), a Ramón y Cajal postdoctoral contract by the Ministerio de Ciencia e Innovación, Spain (RYC-2012-11996), and the collaboration project between Universitat Politècnica de Catalunya- BarcelonaTech and Termo Fluids S.L. DNS calculations have been performed on the IBM MareNostrum supercomputer at the Barcelona Supercomputing Center. The authors thankfully acknowledge these institutions.

REFERENCES

[1] D. Barhaghi, L. Davidson, Natural convection boundary layer in a 5:1 cavity, Physics of Fluids 19 (2007) 125106.

[2] A. Sergent, P. Joubert, S. Xin, P. Le Quéré, Resolving the stratification discrepancy of turbulent natural convection in differentially heated air-filled cavities Part II: End walls effects using large eddy simulation, International Journal of Heat and Fluid Flow 39 (2013) 15–27.

[3] J. Patterson, J. Imberger, Unsteady natural convection in a rectangular cavity, *Journal of Fluid Mechanics* 100 (1980) 65–86.

[4] D. Gray, A. Giorgini, The validity of the Boussinesq approximation for liquids and gases, *International Journal of Heat and Mass Transfer* 19 (1976) 545–551.

[5] P. Le Quéré, Transition to unsteady natural convection in a tall water-filled cavity, Physics of Fluids A 2 (1990) 503–515.

[6] D. Kizildag, I. Rodríguez, A. Oliva, O. Lehmkuhl, Limits of the Oberbeck-Boussinesq approximation in a tall differentially heated cavity filled with water, *International Journal of Heat and Mass Transfer* 68 (2014) 489–499.

[7] R. W. C. P. Verstappen, A. E. P. Veldman, Symmetry-preserving discretization of turbulent flow, *Journal of Engineering Mathematics* 187 (1) (2003) 343–368.

[8] F. X. Trias, A. Gorobets, A. Oliva, A simple approach to discretize the viscous term with spatially varying (eddy-)viscosity. *Journal of Computational Physics*, 253 (2013) 405–417.

[9] F. X. Trias, O. Lehmkuhl, A self-adaptive strategy for the time integration of Navier-Stokes equations, Numerical Heat Transfer, Part B 60 (2) (2011) 116–134.

[10] R. Borrell, O. Lehmkuhl, F. X. Trias, A. Oliva, Parallel direct Poisson solver for discretisations with one Fourier diagonalisable direction, *Journal of Computational Physics*, 230(12) (2011) 4723–4741.

[11] O. Lehmkuhl, C. D. Pérez-Segarra, R. Borrell, M. Soria, A. Oliva, TERMOFLUIDS: A new Parallel unstructured CFD code for the simulation of turbulent industrial problems on low cost PC cluster, in: *Proceedings of the Parallel CFD 2007 Conference*, 2007, pp. 1–8.

[12] F. Nicoud, F. Ducros, Subgrid-scale stress modeling based on the square of the velocity gradient tensor, *Flow, Turbulence and Combustion* 62 (1999) 183–200.

[13] R. Verstappen, When does the viscosity damp subfilter scales sufficiently?, Journal of Scientific Computing 49 (1) (2011) 94–110.

[14] T. J. R. Hughes, L. Mazzei, K. E. Hanzen, Large eddy simulation and the variational multiscale method, Computing and Visualization in Science 3 (1) (2000) 47–59.